Applied Mathematics and Computation 414 (2022) 126660

Contents lists available at ScienceDirect

Applied Mathematics and Computation

journal homepage: www.elsevier.com/locate/amc

Simple and robust contact-discontinuity capturing central algorithms for high speed compressible flows

Ramesh Kolluru [a,b,*], N.V. Raghavendra [a,d], S.V. Raghurama Rao [a], G.N. Sekhar [c]

[a] Department of Aerospace Engineering, Indian Institute of Science, Bangalore, India
[b] Department of Mechanical Engineering, B.M.S.College of Engineering, Bangalore, India
[c] Department of Mathematics, B.M.S.College of Engineering, Bangalore, India
[d] Department of Aeronautical Engineering, Annasaheb Dange College of Engineering, Sangli, Maharastra, India

ARTICLE INFO

Article history:
Received 28 February 2021
Revised 9 September 2021
Accepted 10 September 2021
Available online 9 October 2021

Keywords:
Compressible flow solvers
Rankine-Hugoniot jump condition
Generalised riemann invariants
Robust central schemes
Accurate contact discontinuity capturing
Eigen-structure independence

ABSTRACT

The nonlinear convection terms in the governing equations of compressible fluid flows are hyperbolic in nature and are nontrivial for modelling and numerical simulation. Many numerical methods have been developed in the last few decades for this purpose and are typically based on Riemann solvers, which are strongly dependent on the underlying eigen-structure of the governing equations. Objective of the present work is to develop simple algorithms which are not dependent on the eigen-structure and yet can tackle easily the hyperbolic parts. Central schemes with smart diffusion mechanisms are apt for this purpose. For fixing the numerical diffusion, the basic ideas of satisfying the Rankine-Hugoniot (RH) conditions along with generalized Riemann invariants are proposed. Two such interesting algorithms are presented, which capture grid-aligned steady contact discontinuities exactly and yet have sufficient numerical diffusion to avoid numerical shock instabilities. Both the algorithms presented are robust in avoiding shock instabilities, apart from being accurate in capturing contact discontinuities, do not need wave speed corrections and are independent of eigen-struture of the underlying hyperbolic parts of the systems.

1. Introduction

Development of numerical algorithms for simulating compressible fluid flows is an active area of research. The quest to develop simple, robust and low numerical diffusion algorithms has been a continuing feature of research in CFD in the past several decades. For a detailed review of these schemes the reader is referred to [3,6–9,25,26,18,30]. The features worth considering while developing new schemes for hyperbolic systems representing gas dynamics are a) Exact capturing of steady discontinuities, b) Minimum numerical diffusion without violating entropy conditions, c) Avoiding shock instabilities d) Eigen-structure independency and simplicity of the algorithm. Most popular algorithms depend on Riemann solvers and eigen-structure. Though some of them can capture grid aligned steady shocks or contact-discontinuities exactly, they often produce unphysical phenomena like carbuncle shocks, kinked Mach stems, odd-even decoupling, and violation of entropy conditions, because of inherent low numerical diffusion present in them. Researchers in the recent past have focused on algorithms which can avoid these anomalies and the search for an ideal scheme is still continuing. In this quest, it will be

* Corresponding author.
E-mail addresses: kollurur@iisc.ac.in, rameshkolluru43@gmail.com (R. Kolluru), venkata.r.nandagiri@gmail.com (N.V. Raghavendra), raghu@iisc.ac.in, svraghuramarao@gmail.com (S.V. Raghurama Rao), gnsbms@gmail.com (G.N. Sekhar).

https://doi.org/10.1016/j.amc.2021.126660
0096-3003/

advantageous to incorporate the physical and mathematical features characteristic of the nonlinear propagating waves. Out of the three nonlinear waves, the shock waves must satisfy the Rankine-Hugoniot conditions, the rarefaction waves must satisfy the Generalized Riemann Invariants (GRI) and the contact-discontinuities must satisfy both [30]. In the present work we use both the above criteria to develop two new, simple and robust algorithms for Euler and Navier-Stokes equations. The framework of central solvers is taken as the foundation for the sake of simplicity. For a detailed review of central discretization schemes the reader is referred to [8,9,24]. Within the framework of central solvers, the focus of this research work is on accurate capturing of contact discontinuities, capturing them exactly in steady state. Additionally, the motivation is also to develop accurate central solvers that do not depend on eigen-structure of the underlying systems.

The rest of the paper is organized as follows. In Section 2 a brief introduction for the governing equations and time discretization in finite volume framework is presented. The description of the new algorithms is presented in sections 3 and 4. In Sections 5 and 7, the results produced by these new robust algorithms for various 1D and 2D bench-mark test cases both for Euler and Navier Stokes equations are presented, followed by a summary in the last section.

2. Governing equations

The basic equations are unsteady compressible Navier-Stokes equations for viscous flows and Euler equations for inviscid flows with perfect gas EOS as described in [24]. In this work cell centred finite volume framework is used to discretize both Euler and NS equations and are solved using TVD RK for time discretisation method as given in (1) [6] where $\overline{U}$ represents cell integral average of the conserved variable vector and R represents the residue of fluxes for a given cell (i,j).

$$\begin{aligned}
\overline{U}_{ij}^{1} &= \overline{U}_{ij}^{n} - \Delta t R_{ij}^{n}\left(\overline{U}_{ij}^{n}\right) \\
\overline{U}_{ij}^{2} &= \tfrac{1}{4}\overline{U}_{ij}^{1} + \tfrac{3}{4}\overline{U}_{ij}^{n} - \tfrac{1}{4}\Delta t R_{ij}\left(\overline{U}_{ij}^{1}\right) \\
\overline{U}_{ij}^{n+1} &= \tfrac{2}{3}\overline{U}_{ij}^{2} + \tfrac{1}{3}\overline{U}_{ij}^{n} - \tfrac{2}{3}\Delta t R_{ij}\left(\overline{U}_{ij}^{2}\right)
\end{aligned} \tag{1}$$

In order to obtain higher order accuracy in space the solution is reconstructed using limiter based reconstruction process as given in (2) [13].

$$\begin{aligned}
U(x,t^n) &= \left[U_i^n + \left(\frac{\partial U}{\partial x}\right)_i (x - x_i)\right], \\
\left(\frac{\partial U}{\partial x}\right)_i &= minmod\left[\zeta\frac{U_{i+1}-U_i}{\Delta x}, \zeta\frac{U_i - U_{i-1}}{\Delta x}, \frac{U_{i+1}-U_{i-1}}{2\Delta x}\right], 1 \le \zeta \le 2 \\
&\quad (\text{or}) \\
\left(\frac{\partial U}{\partial x}\right)_i &= minmod\left[\zeta\frac{U_{i+1}-U_i}{\Delta x}, \zeta\frac{U_i - U_{i-1}}{\Delta x}\right], 0 \le \zeta \le 1
\end{aligned} \tag{2}$$

3. Riemann Invariant Based Contact-Discontinuity Capturing Algorithm (RICCA)

In this section a novel scheme is presented in which the effect of Generalized Riemann Invariants is utilized in the discretization process, leading to a scheme which captures steady contact discontinuities exactly.

3.1. Generalised Riemann Invariants (GRI)

The concept of GRI is briefly introduced here (for a more detailed explanation see [10,28,30]). Consider a general quasi-linear hyperbolic system as given by (3).

$$\frac{\partial U}{\partial t} + A(U)\frac{\partial U}{\partial x} = 0, \tag{3}$$

$$U = [U_1, U_2, \cdots, U_m]^T, \tag{4}$$

where U represents the conserved variable vector of the hyperbolic system. Of the m waves associated with the system (3) for the i^{th} characteristic field associated with eigenvalue λ_i, corresponding right eigenvector is given by

$$\mathbf{R^i} = \left[\mathbf{r_1^i}, \mathbf{r_2^i} \cdots \mathbf{r_m^i}\right]^{\mathbf{T}} \tag{5}$$

The Generalised Riemann Invariants are relations that hold true across expansion waves and contact-discontinuites. This can be mathematically written as

$$\frac{dU_1}{\mathbf{r_1^i}} = \frac{dU_2}{\mathbf{r_2^i}} = \cdots = \frac{dU_m}{\mathbf{r_m^i}} \tag{6}$$

These equations relate ratios of dU_j to the respective component r_i^j of the right eigenvector R_i^j, corresponding to an eigenvalue λ_i. Here, the above relations (GRIs) are utilised in developing a new algorithm which can recognise contact-discontinuities and the algorithm is expected to be accurate enough for flow simulations. The above ideas will be incorporated in a simple central discretisation framework in the finite volume method, avoiding Riemann solvers, field-by-field decompositions and complicated flux splittings. This is achieved by fixing the coefficient of numerical diffusion in a generic expression for the interface flux based on the above criteria.

3.2. A central solver based on GRI

The finite volume update formula for Euler equations is given by (7) with interface flux evaluated as in (8).

$$\bar{U}_j^{n+1} = \bar{U}_j^n - \frac{\Delta t}{\Delta x}\left[F_{j+\frac{1}{2}}^n - F_{j-\frac{1}{2}}^n\right] \tag{7}$$

$$F_{j\pm\frac{1}{2}} = F_I(U_L, U_R) = \frac{1}{2}[F(U_L) + F(U_R)] - \frac{|\alpha_I|}{2}\Delta U \tag{8}$$

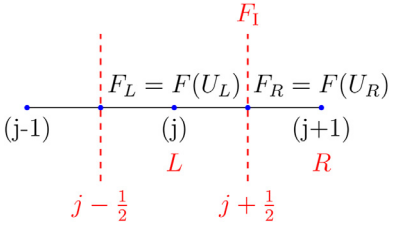

Fig. 1. Typical finite volume in 1D.

The first term on the right hand side is an average flux from the left (L) and the right (R) states of an interface (I) and the second term is numerical diffusion. Here a diagonal matrix is assumed for α_I, as in [8]. Various numerical schemes differ in the way this wave speed or the coefficient of numerical diffusion is determined. The basic idea of the present work is to use GRI across the interface to determine the coefficient of diffusion, α_I. As shown [28,30], a contact-discontinuity separates two states in a linearly degenerate field and constancy of the GRI holds good across this wave, apart from R-H conditions. The GRIs (6) applied to the contact-discontinuity leads to the following ODEs:

$$\frac{d\rho}{1} = \frac{d(\rho u)}{u} = \frac{d(\rho E)}{\frac{u^2}{2}}. \tag{9}$$

Solving the above ODEs (9) results in pressure and velocity being constant across a contact-discontinuity [28,30]. Therefore the conditions for pressure and velocity across the cell interface can be written as (10)

$$\begin{aligned} \Delta u &= 0 \text{ or } u_j = u_{j+1} = u_I, \\ \Delta p &= 0 \text{ or } p_j = p_{j+1} = p_I. \end{aligned} \tag{10}$$

Using the conditions (10) in the expressions of $(\alpha_I)_l, \quad l = 1, 2, 3$, one can obtain the following.

$l = 1$:.

$$(\alpha_I)_1 = \left|\frac{(F_1)_{j+1} - (F_1)_j}{(U_1)_{j+1} - (U_1)_j}\right| = \left|\frac{\rho_{j+1}u_{j+1} - \rho_j u_j}{\rho_{j+1} - \rho_j}\right| = |u_I| \tag{11}$$

$l = 2$:

$$(\alpha_I)_2 = \left|\frac{(F_2)_{j+1} - (F_2)_j}{(U_2)_{j+1} - (U_2)_j}\right| = \left|\frac{p_{j+1} + \rho_{j+1}u_{j+1}^2 - p_j - \rho_j u_j^2}{\rho_{j+1}u_{j+1} - \rho_j u_j}\right| = |u_I| \tag{12}$$

$l = 3$:

$$(\alpha_I)_3 = \left|\frac{(F_3)_{j+1} - (F_3)_j}{(U_3)_{j+1} - (U_3)_j}\right| = \left|\frac{p_{j+1}u_{j+1} + \rho_{j+1}u_{j+1}E_{j+1} - p_j u_j - \rho_j u_j E_j}{\rho_{j+1}E_{j+1} - \rho_j E_j}\right| = |u_I| \tag{13}$$

From the above three expressions the coefficient of numerical diffusion determined to accurately capture contact-discontinuity located at the cell interface $I \equiv j + \frac{1}{2}$ is

$$(\alpha_I)_l = |u_I|, \quad l = 1, 2, 3 \tag{14}$$

leading a scalar numerical diffusion. Using (10), the above coefficient of diffusion can be expressed in four different ways as

$$(\alpha_I)_l = |u_j| = |u_{j+1}| \text{ or } (\alpha_I)_l = \frac{|u_j| + |u_{j+1}|}{2} \text{ or } (\alpha_I)_l = max(|u_j|, |u_{j+1}|), \quad l = 1, 2, 3. \tag{15}$$

In a general multi-dimensional flow case, the coefficient of numerical diffusion to accurately capture a contact-discontinuity can be expressed as

$$\alpha_I = |V_{nL}| = |V_{nR}| = \frac{|V_{nL}| + |V_{nR}|}{2} = max(|V_{nL}|, |V_{nR}|), \tag{16}$$

which V_n is normal interface velocity. Numerical experimentation has revealed that, this numerical diffusion evaluated by (15) or (16), though adequate in capturing the contact-discontinuities exactly, is not sufficient enough for the case of shocks being located at the cell interface. So in order to generalize the diffusion for any case the Riemann Invariant based Contact-discontinuity Capturing Algorithm (RICCA) is designed with the following coefficient of numerical diffusion:

$$\alpha_I = \begin{cases} \frac{|V_{nL}|+|V_{nR}|}{2}, & \text{if } |\Delta \mathbf{F}| < \delta \text{ and } |\Delta \mathbf{U}| < \delta \\ max(|V_{nL}|, |V_{nR}|) + sign(|\Delta p_I|)a_I, & \text{otherwise} \end{cases} \tag{17}$$

A value of 1×10^{-8} is used for δ for all the test cases. Here, $a_I = \sqrt{\frac{\gamma p_I}{\rho_I}}$ is the speed of sound evaluated with the values at the interface given by

$$\rho_I = \frac{\rho_L + \rho_R}{2}, \tag{18}$$

$$p_I = \frac{p_L + p_R}{2}, \tag{19}$$

$$\Delta p_I = (p_R - p_L). \tag{20}$$

From (17) it can be seen that for the case of a steady contact-discontinuity at the interface where $sign(|\Delta p_I|) = 0$, the coefficient α_I becomes identical to the expression in (16) resulting in exact capturing of the steady contact-discontinuity. On the other hand, if a shock is located at the interface in which case $sign(|\Delta p_I|) = 1$, the expression for the coefficient in (17) becomes $max(|V_{nL}|, |V_{nR}|) + a_I$ which is a Rusanov (LLF) type diffusion and should be adequate near shocks. Even in the case of an expansion region with a sonic point ($M = 1$) at the interface, $sign(|\Delta p_I|) = 1$, the expression for the coefficient in (17) becomes $max(|V_{nL}|, |V_{nR}|) + a_I$ which results in non-zero diffusion ensuring no expansion shocks. So, entropy violation is unlikely to occur. This design of the coefficient of numerical diffusion therefore does not require any entropy fix.

On the whole, the new central scheme RICCA a) can capture steady grid-aligned contact-discontinuities exactly, b) has sufficient numerical diffusion near shocks so as to avoid shock instabilities, c) does not need entropy fix for at sonic points d) is not tied down to the eigen-structure, e) hence can be easily extended to any general equation of state, without modification. A similar strategy was introduced by N.V. Raghavendra in [31] to design an accurate contact-discontinuity capturing discrete velocity Boltzmann scheme for inviscid compressible flows.

4. New central scheme, MOVERS+

The second of the two new algorithms presented in this paper is based on subtantial modification of a central Rankine-Hugoniot solver developed by Jaisankar & Raghurama Rao [8], called as MOVERS (Method of Optimal Viscosity for Enhanced Resolution of Shocks). MOVERS [8] requires wave speed correction in order to restrict the coefficient of diffusion to within the eigenspectrum. To avoid wave speed correction, a simpler strategy is proposed in this section which is described below.

$$d_{I,j} = \frac{1}{2}\left|\frac{\Delta F_j}{\Delta U_j}\right|\Delta U_j, \quad j = 1, 2, 3 \tag{21}$$

$$= \frac{1}{2}\frac{\left|\Delta F_j\right|}{\text{sign}(\Delta U_j)\Delta U_j}\Delta U_j \tag{22}$$

$$= \frac{1}{2}\,\text{sign}(\Delta U_j)\left|\Delta F_j\right|, \quad j = 1, 2, 3 \tag{23}$$

where the relation $\frac{1}{\text{sign}(\cdot)} = \text{sign}(\cdot)$ is used. This form of d_I will eliminate the need for wave speed correction is MOVERS. Numerical experimentation has revealed that this numerical scheme has very low diffusion and captures steady discontinuities exactly but encounters problems in smooth regions due to lack of sufficient numerical diffusion. Therefore, using a shock sensor (25), an additional numerical diffusion is introduced. This additional diffusion is based on the fluid velocity, which is demonstrated to be sufficient to avoid unphysical expansions in smooth regions [24]. The coefficient of numerical diffusion for MOVERS+ is given by

$$|d_I|_j = \frac{\Phi}{2}Sign(\Delta U_j)|\Delta F_j| + \left(\frac{|V_{nL}| + |V_{nR}|}{2}\right)\Delta U_j, \quad j = 1, 2, 3 \tag{24}$$

where the Φ is the shock sensor defined by

$$\Phi = \left| \frac{\Delta p}{2 p_I} \right| \text{ with } p_I = \frac{p_L + p_R}{2} \tag{25}$$

The features of this modified algorithm, MOVERS+, are as follows, a) It can capture steady grid-aligned contact discontinuities exactly and provides low diffusion otherwise, b) It has sufficient numerical diffusion near shocks so as to avoid shock instabilities (deliberately giving up exact shock capturing of MOVERS for gain in robustness), c) It does not need entropy fix for smooth regions or in expansion regions, d) It does not require any wave speed correction, unlike in MOVERS, e) It is a simple central solver and is not based on Riemann solvers, field-by-field decompositions or complicated flux splittings, thus making it a suitable candidate for extending it to real gas EOS, multiphase and multicomponent flows without any modifications [24].

5. Results and discussion

To test the accuracy and robustness of the numerical schemes RICCA and MOVERS+, results from various 1-D and 2-D benchmark cases are presented in the following sections.

5.1. 1-D Shock tube problems

These are robustness and accuracy test problems with initial conditions as specified in chapter 4 of [23] and [30]. Both the schemes RICCA and MOVERS+ are tested for: Sod test problem with a sonic point, a strong shock, strong rarefaction, slowly-moving shock and slowly-moving contact-discontinuity and their interactions. The initial conditions for these test cases are given in the Table 1. For all the test cases that are being considered in 1D a total of 100 computation cells are considered and the CFL number, unless and otherwise specified, is taken as 0.1. Numerical results are compared with the analytical solutions of the Riemann problems.

Test case 1 corresponds to a Sod shock tube problem with mild shock strength. This test case has an expansion fan (containing a sonic point) moving to the left, a shock moving towards right side and a contact-discontinuity in between these two. Typically low diffusion schemes encounter problems in the expansion fans, especially at sonic points. MOVERS-n gives a small non-smooth variation near the sonic point while Roe scheme yields a large and unphysical expansion shock, as shown in figure (2 a). It can be observed from figure (3-a) that both RICCA and MOVERS+ do not produce expansion shocks or non-smoothness in the expansion region. It can be seen from the (3-a) there is a small glitch for HLLC which is also evident in solution from page no 337 of [30]. Further, It can be observed that RICCA is more diffusive in shock capturing when compared to MOVERS+, which is also seen in many other test cases described in this section.

Table 1
Initial conditions for 1D test cases as given in [30].

Case	ρ_L	p_L	u_L	ρ_R	p_R	u_R
1	1.0	1.0	0.0	0.125	0.1	0.0
2	1.0	0.4	-2.0	1.0	0.4	2.0
3	1.0	1000.0	0.0	1.0	0.01	0.0
4	1.0	0.01	0.0	1.0	100.0	0.0
5	5.99924	460.894	19.5975	5.99242	46.0950	-6.19633
6	1.0	$\frac{1}{\gamma M^2}$	1.0	$\frac{\frac{\gamma+1}{\gamma-1}\frac{p_R}{p_L}+1}{\frac{\gamma-1}{\gamma+1}+\frac{p_R}{p_L}}$	$p_L \frac{2\gamma M^2-(\gamma-1)}{\gamma+1}$	$\sqrt{(}\gamma \frac{(2+(\gamma-1)M^2)p_R}{(2\gamma M^2+(1-\gamma))\rho_R})$
7	1.4	0.4	0.0	1.0	0.4	0.0
8	1.4	1.0	0.1	1.0	1.0	0.1
9	3.86	10.33	-0.81	1.0	1.0	-3.44

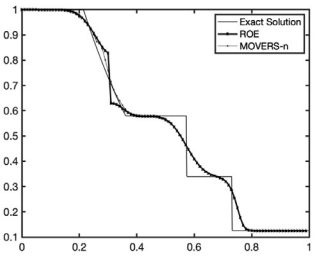

(a) Non-smoothness in expansion and expansion shock

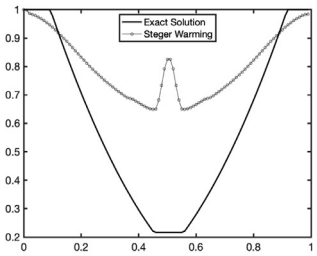

(b) Internal energy plot for Toro test case 2

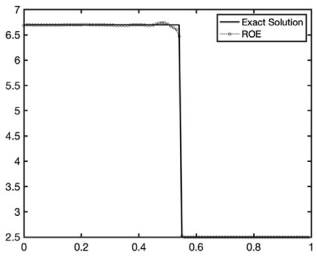

(c) Post shock oscillations in Slowly moving shock

Fig. 2. General Issues with popular schemes.

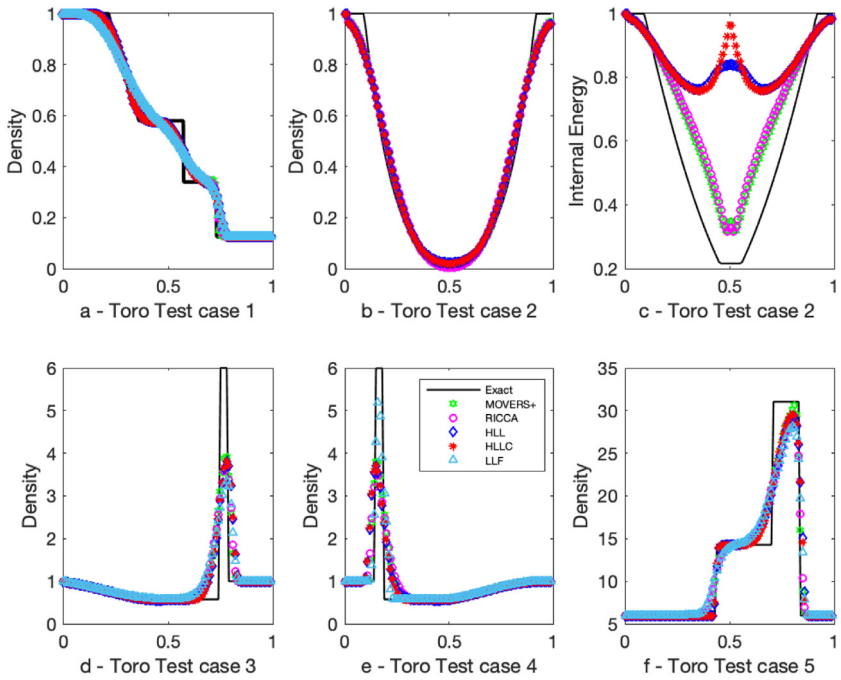

Fig. 3. Density for Toro Test cases 1 to 5.

Test case 2, also known as *123 problem*, consists of two strong and symmetric rarefactions approaching each other and a trivial contact-discontinuity of zero wave speed between them. The pressure between these rarefactions can go as low as zero (close to vacuum). This test case can also be considered as a benchmark test case for low density flows. Many low diffusion schemes fail for this case. Other numerical schemes would give a wrong value of internal energy as shown in figure (2 b). Hence the schemes which can resolve this test case are considered to be robust. Figures (3 - b,3 - c) shows the results obtained by LLF, HLL, HLLC, MOVERS+ and RICCA respectively. The ability of a numerical scheme to capture the low density is tested in this test case. Both the new numerical schemes can capture the low pressure and density regions close to vacuum. Also the prediction of internal energy by RICCA and MOVERS+ is much better than other schemes. Test case 3 represents a strong and severe problem, designed to test the robustness and accuracy of numerical schemes. It consists of a left rarefaction, a contact-discontinuity and a strong right shock wave with shock Mach number 198. This test case forms the left half portion of the blast wave problem of Woodward and Colella [32]. Figures (3-d,3-e) represents solutions obtained from LLF, HLL, HLLC, MOVERS+ and RICCA. Both the numerical schemes are capable of capturing strong shocks. Test case 5 represents another difficult problem, which is taken from the right half of the Woodward and Colella [32] problem. This problem consists of a left shock, a contact-discontinuity and a right rarefaction. Figure (3-f) represent the solutions of the test case 5 using HLL, HLLC, MOVERS+ and RICCA respectively. Test case 6 is designed to mimic the conditions of a shock in steady state [34]. Initial conditions for the this test case are given in the table (1). MOVERS-n and Roe schemes capture steady shock exactly. Figure (4-b) represents the results for steady state shock using MOVERS+ and RICCA. Both the numerical schemes diffuse the steady shock. This is expected, as the exact shock capturing is deliberately given up in the designing of the schemes for avoiding shock instabilities, still retaining exact contact discontinuity capturing. Both numerical schemes are designed to capture the steady state contact-discontinuities exactly similar to HLLC scheme. In order to check this capability, test case 7 is designed to specifically mimic a steady state contact-discontinuity. It is a known fact that across this discontinuity there will be no variation in pressure and velocity but density variation occurs. Both these schemes have the ability to capture steady contact-discontinuity exactly as shown in figure (4-a).

Typically low diffusive schemes will generate oscillations near slowly moving shocks and contact discontinuities, as shown in (2 c) and as described in [11,23,29]. Fig. (5) represents solutions obtained by MOVERS+ and RICCA which show no such oscillations.

5.2. 2-D Euler test cases

In this section the numerical schemes described in the sections (3,4) are tested on typical benchmark test case for 2-D Euler equations. Robustness and accuracy of the schemes RICCA and MOVERS+ are thoroughly explored using various test cases. These cases are primarily used to evaluate the performance of the numerical schemes. For steady state problems the solutions are shown when the relative error is dropped to machine epsilon or when the code is run to 100,000 iterations.

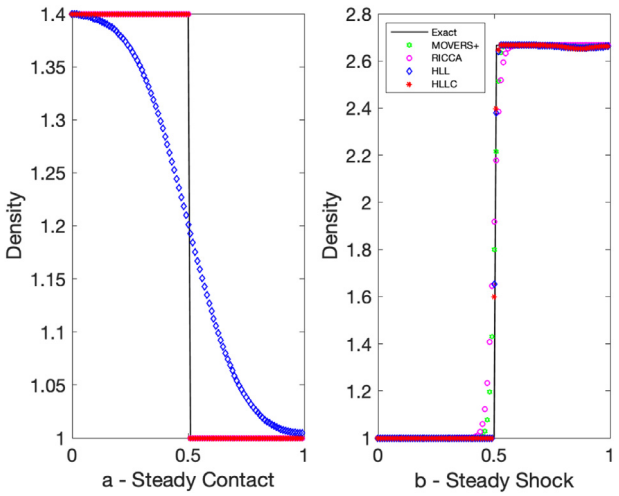

Fig. 4. Steady state shock and Steady state contact discontinuity.

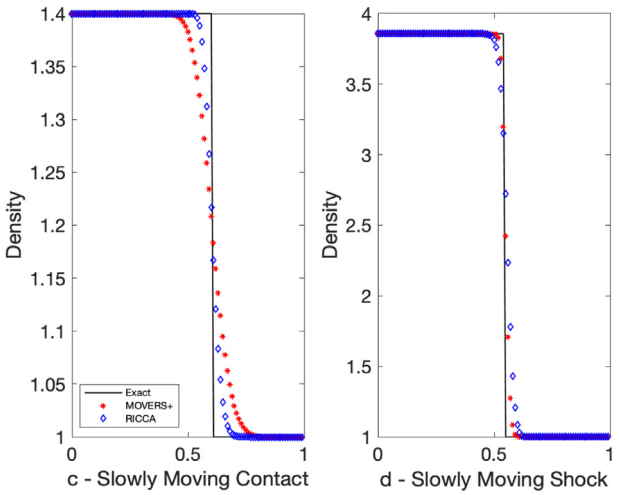

Fig. 5. Slowly moving Contact discontinuity and Shocks.

Each problem is run on a minimum of three sets of grids and the finest grid solutions are presented for all the test cases. The steady sate test cases considered are a) Oblique shock reflection b) Supersonic flow over 15° compression ramp c) Horizontal slip flow, d) Supersonic flow over a thick bump, e) Supersonic flow over forward-facing step. The second set of test cases are used to test the anomalies like carbuncle, odd even decoupling, which are not admissible and are commonly found in low diffusive algorithms. These test cases are a) Hypersonic flow past a half-cylinder, b) Odd Even Decoupling Problem, c) Shock Diffraction and d) Double Mach Reflection.

5.2.1. Oblique shock reflection

This test case [33] describes an oblique shock hitting a flat plate and getting reflected. The computational domain considered for this test case is $[0, 3] \times [0, 1]$. An oblique shock with the incident shock angle of 29° and the free stream Mach number $M = 2.9$ is introduced from the left-top corner of the computational domain. The details of boundary conditions and initial conditions are explained in detail in [24]. Three standard grid sizes (120×40, 240×80 and 480×160) are considered for the study. Figures (6) shows the second-order accurate solutions of both RICCA and MOVERS+ on the fine grid. Both the schemes, RICCA and MOVERS+, are capable of resolving incident and reflected shocks well. The convergence plots of second order MOVERS+ and RICCA are shown in the figure (7). It can be observed that RICCA converges to machine epsilon whereas MOVERS+ converges to 1×10^{-5}.

5.2.2. Supersonic flow over a 15° compression ramp

This is the case of a supersonic flow over a 15° degree ramp [15] placed in a wind tunnel. The computational domain consists of the following dimensions $[0, 3] \times [0, 1]$ with supersonic inlet, supersonic exit and flow tangency wall boundary

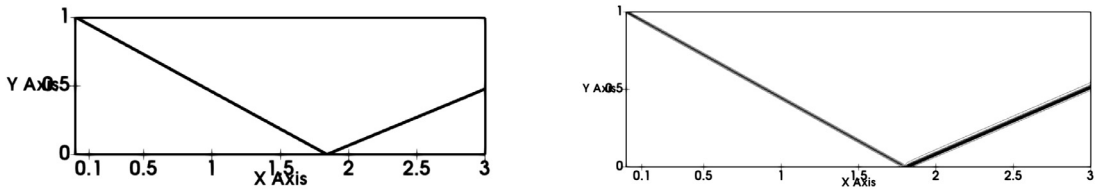

(a) Movers+ on grid Size 480 × 160 (b) RICCA on grid Size 480 × 160

Fig. 6. Pressure Contours (0.71:0.1:2.91) - for regular shock reflection; second order Results.

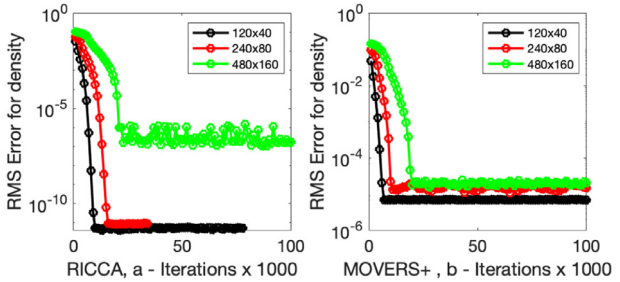

Fig. 7. Convergence plot of MOVERS+ and RICCA on all grids.

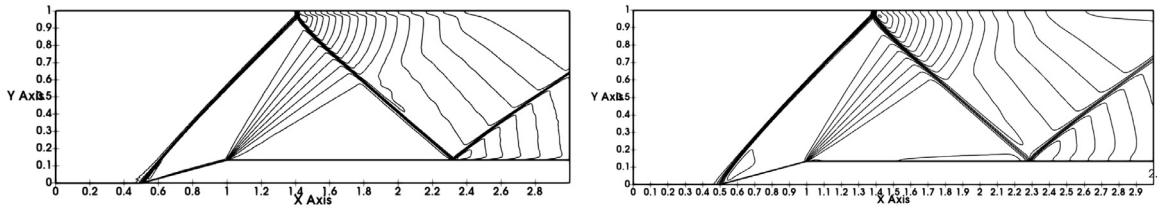

(a) MOVERS+ on grid Size 480 × 160 (b) RICCA on grid Size 480 × 160

Fig. 8. Density Contours (0.85:0.095:2.75) - for 15° Ramp second order Results.

conditions applied. As a supersonic flow with Mach number $M = 2.0$ approaches this ramp, an oblique shock emerges from the lower end corner (compression corner) of the ramp and an expansion fan emerges from the upper corner (expansion corner) of the ramp. The oblique shock emerging from the compression corner at the beginning of the ramp reflects from the upper wall. The reflected shock interacts with the emerging expansion fan and further gets reflected from the bottom wall. Following grid sizes are used in the numerical simulation: 120×40, 240×80 and 480×160. Figure (8) show the second order accurate results for MOVERS+ and RICCA on 480×160 grid. It is observed that the second order results of MOVERS+ on coarse grid are comparable with the second order results of RICCA on fine grid, though not shown here.

5.2.3. Horizontal slip flow

In this test case [17], a Mach 3.0 flow slips over a Mach 2 flow with no change in pressure and density across the interface. Since the flow features sought are at steady state conditions, the code is run till the relative error reaches machine epsilon or the number of iterations reaches 100000. This problem tests the accuracy of a numerical scheme in resolving a contact discontinuity. Many of the central and upwind schemes diffuse the contact discontinuity, due to high numerical diffusion. The solution of a typical diffusive scheme (Rusanov or LLF method) is shown in the Fig. (9 a). Figs. (9 b) and (9 c) show the second order accurate solutions obtained with MOVERS+ and RICCA. Both RICCA and MOVERS+ capture the grid-aligned slipstream exactly. Though not shown here, even their first order versions resolve it exactly.

5.3. Supersonic inviscid flow over a bump

In this test case [19], supersonic flow at Mach number 1.6 is considered over a 4% thick bump in a channel. The computational domain considered for this test case is $[0, 3] \times [0, 1]$ and three different grid sizes, 300×100, 600×200 and 900×300, are used to test both MOVERS+ and RICCA. As the supersonic flow passes the bump, oblique shocks evolve from the leading edge and trailing edge of the bump. Further, the leading edge shock hits the top wall and reflects back, leaving out of the domain. It can be observed that the evolution of shocks and their interactions are well captured by both the schemes, RICCA and MOVERS+.

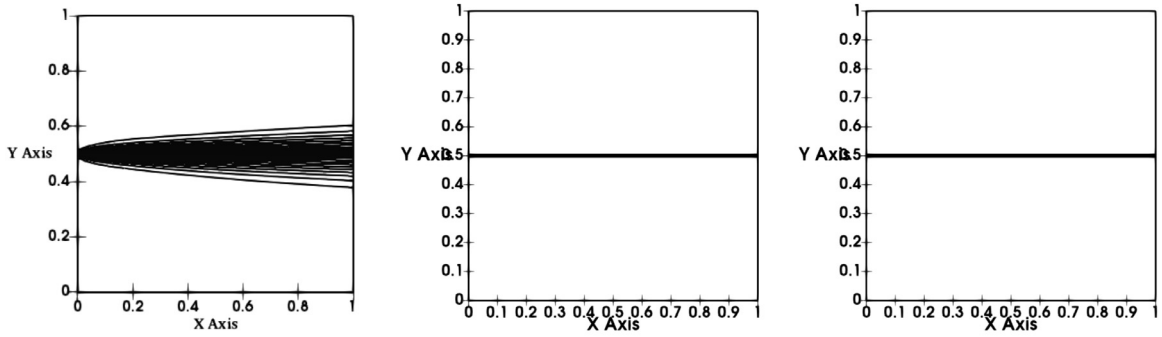

(a) LLF 2O Result (b) MOVERS+ (c) RICCA

Fig. 9. Second-order- Mach Contours (2:0.033:3) - for Slip Flow on a 100 × 100 grid.

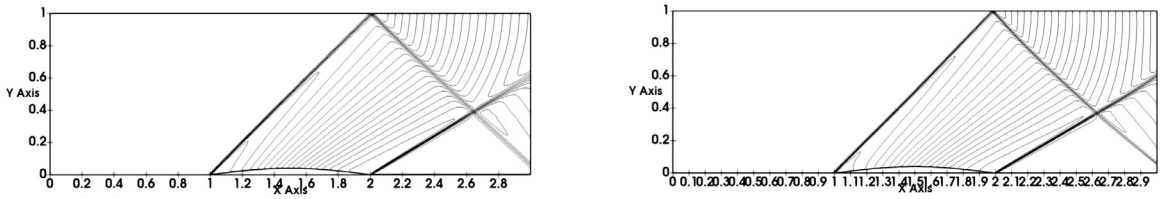

(a) Movers+ on grid size 900 × 300 (b) RICCA on grid size 900 × 300

Fig. 10. Density Contours for flow over bump.

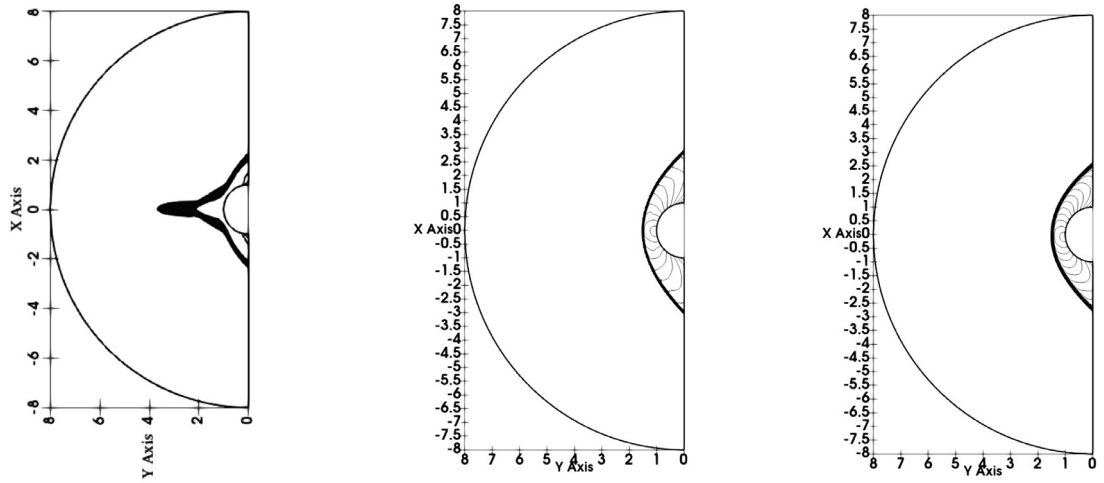

(a) ROE Scheme (b) MOVERS+ (c) RICCA

Fig. 11. Comparison of 2O solutions of ROE scheme with RICCA and MOVERS+ for carbuncle effect on 480 × 160 Grid.

5.3.1. Hypersonic flow past a half-cylinder

This test case assesses a numerical scheme for the shock instability called carbuncle shock discussed by Quirk [23] and Meng-Sing Liou [16]. A hypersonic flow of $M = 6$ over a half cylinder leads to a detached bow shock in front of the bluff body. Many of the approximate Riemann solvers like Roe scheme and low diffusive schemes produce carbuncle shocks as shown in figure (11 a). Second order (2O) accurate solutions of RICCA and MOVERS+ are compared with that of 2O solution of Roe Scheme on a 480 × 160 grid in figures (11 b) and (11 c). It can be observed from Fig. (11), that MOVERS+ and RICCA capture the bow shock without producing carbuncle shocks. MOVERS+ is shown to produce a crisper shock compared to RICCA.

5.3.2. Shock diffraction

This is another test case [4] which assesses a numerical scheme for shock instability resulting in shock anomalies and expansion shock as described in [23]. This test case has complex flow features involving a planar shock wave moving with

(a) MOVERS+ (b) RICCA

Fig. 12. Contours of Density at time=0.1561 - for shock diffraction test case on a 1280×1280 grid using MOVERS+ and RICCA.

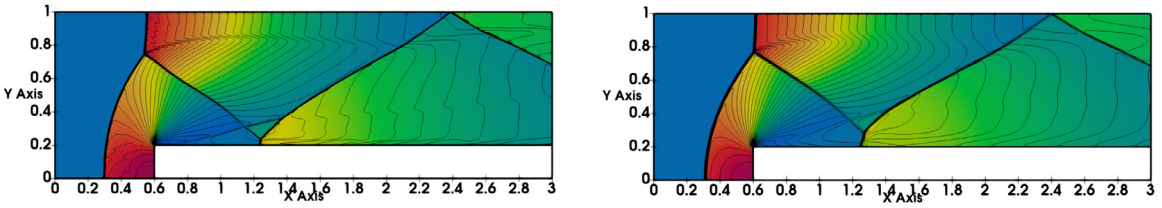

(a) MOVERS+ (b) RICCA

Fig. 13. Second-order results with MOVERS+ and RICCA on 960×320 Grid.

incident Mach number 5.09, a diffracted shock wave around the 90° corner and a strong expansion wave. The strong shock wave accelerates the flow and interacts with strong expansion to further complicate the flow. Other distinct flow features are a slipstream and a contact surface. Godunov and Roe schemes are known to fail for this test case [23] as they admit expansion shocks without a proper fix. Second order results for this unsteady test case (at time t=0.1561) are presented in figure (12). Both MOVERS+ and RICCA do not produce expansion shocks for this test case.

The features of the solution for the strong strong diffraction case are explained clearly in [27]. It can be observed that the slipstream, the triple point near the lower edge and other shock structures are all well resolved by MOVERS+ than RICCA. Further, the solution accuracy of MOVERS+, presented on 1280×1280 grid in figure (12), is comparable with the solution presented in refernce [20] on a 1280×1280 simulated with modified HLLC and with WENO scheme of 5^{th} order.

5.3.3. Supersonic flow over a forward-facing step

In this unsteady test case [32], a Mach 3 flow enters a wind tunnel containing a forward-facing step. The computational domain ($[3, 0] \times [0, 1]$) consists of a step size of 0.2 units begining at $x = 0.6$. Grid sizes of 120×40, 240×80, 480×160 and 960×320 are used in the simulations. As the test case is an unsteady one, the results at time t=4.0 are presented for the fine grid. At $t = 4.0$, a lambda shock is developed and a slipstream can be seen emanating from the triple point. Results are presented with second-order accuracy in figure (13) for both MOVERS+ and RICCA on a 920×360 grid. Both the numerical schemes MOVERS+ and RICCA resolve the lambda shock and the reflected shocks reasonably well while MOVERS+ resolves the slipstream more accurately.

5.3.4. Odd-even decoupling

This is a testcase described in [23] which assesses a numerical scheme for shock instability called odd-even decoupling. In this test case a slowly moving planar shock with Mach number $M = 6$ simply travels along a long rectangular duct. The ability of the numerical schemes to avoid a numerical instability if the grid is perturbed is tested in this problem. For numerical solution, the duct is set up with a grid size of 800×20 unit square cells and the centerline of the grid is perturbed in the following manner:

$$y_{i,j_{mid}} = \begin{cases} y_{i,j_{mid}} + 10^{-3} \text{ for } i \text{ even}, \\ y_{i,j_{mid}} - 10^{-3} \text{ for } i \text{ odd} \end{cases}$$

Most of the low diffusion schemes distort the shock structure as shown in figure (14 a) because of the perturbed grid. For schemes like Godunov's exact Riemann solver and approximate Riemann solver of Roe, this perturbation promotes odd-even decoupling thereby destroying the planar shock structure [23]. Figures (14 b) and (14 c) represent the 2O solution using

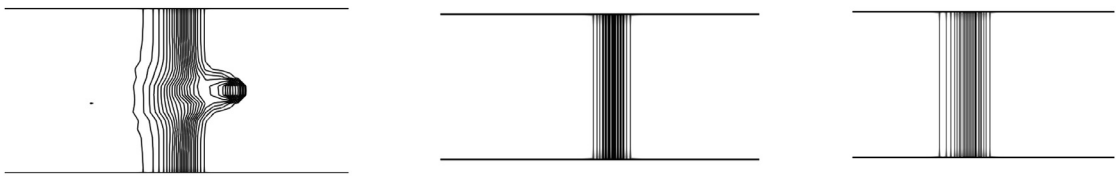

(a) Odd even decoupling by 1O Roe scheme (b) MOVERS+ 2O Results (c) RICCA 2O Results

Fig. 14. Results for odd-even decoupling testcase, density contours on a 800×20 grid at time t=100.

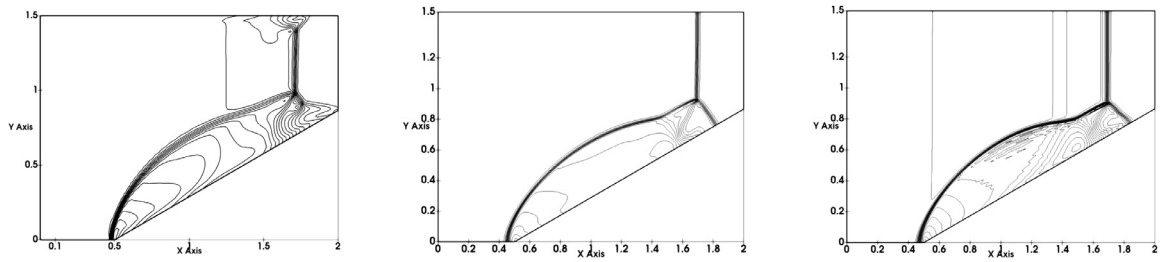

(a) Kinked mach stem using 1O Roe scheme (b) RICCA 2O (c) MOVERS+ 2O

Fig. 15. Density contours (0.98:0.6328:16.8) at time=0.3 - for double-mach reflection on a 240×180 grid.

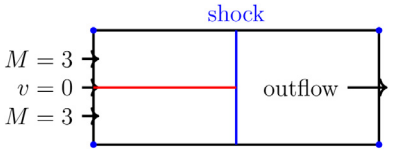

Fig. 16. Vortex shock interaction test case.

MOVERS+ and RICCA. It can be observed that the shock captured (after a long time t=100) using both the schemes are stable to the perturbation and no distortion of the shock structure is seen in these two schemes.

5.3.5. Double-mach reflection (DMR)

In this unsteady test case [32], a Mach 10 shock is driven down a channel containing a 30° wedge. At first the simple planar shock meets the walls of the channel at right angles, but on encountering the sloping surface of the wedge, a complicated shock reflection occurs resulting in the formation of reflected shocks, Mach stems, triple points and slipstreams. A shock-instability termed kinked Mach stem [23] is produced by some schemes as shown in figure (15). Results for this unsteady test case (at time t=0.3) are presented with second-order accuracy in figure (15 b,15 c). Both MOVERS+ and RICCA do not produce kinked Mach stems in capturing various features of double Mach reflection.

6. Vortex shock interaction

Elling [2] has investigated the effect of vortex filament on the shock profile in supersonic flow. This test case is designed to check the ability of the numerical schemes to resolve the physical carbuncles in shock - vortex and/or shock - boundary layer interactions. According to the reference [14], if a numerical scheme fails to resolve this test case then some flow features in shock - boundary layer interaction problems and shock - vortex interaction problems would be missed. This test consists of a channel with coordinates $[0, 100] \times [0, 40]$ equally divided by 100×40 grid points. The domain is initialized with a supersonic flow, with steady shock conditions pertaining to $M = 3$ in the left half of the domain and post shock conditions in the right half. A vortex filament is mimicked by enforcing the velocity to be zero in the upstream conditions at the mid point in y-axis as shown in the Figure (16). Flow tangency boundary conditions are assigned to the top and bottom walls, supersonic exit boundary condition is prescribed at the exit and steady state shock conditions with zero filament velocity is prescribed at the inlet boundary.

Numerical simulations are carried out using LLF, MOVERS+ and RICCA to check if they can resolve the physical carbuncle. As can be seen in the figures (17 a,17 b,17 c) both RICCA and MOVERS+ resolve the physical carbuncle well, much better than LLF. It can also be observed that MOVERS+ is less diffusive when compared to RICCA and LLF, which is evident in resolving the features in figure (17 b).

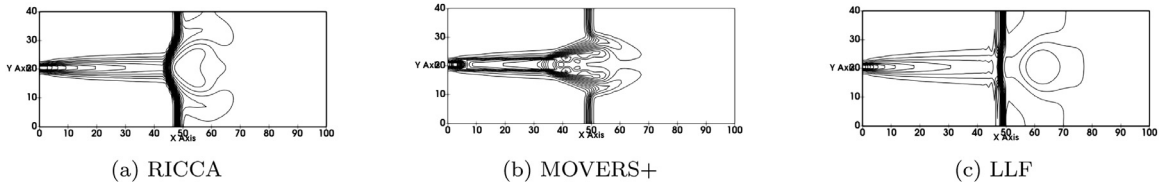

Fig. 17. Entropy contours for vortex shock interaction with M = 3 on a 100×40 grid at t = 100.

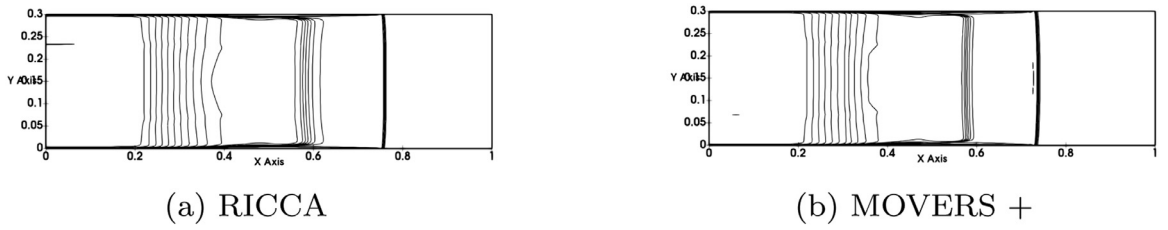

Fig. 18. Density Contours in Viscous Shock Tube on 500×500 Grid.

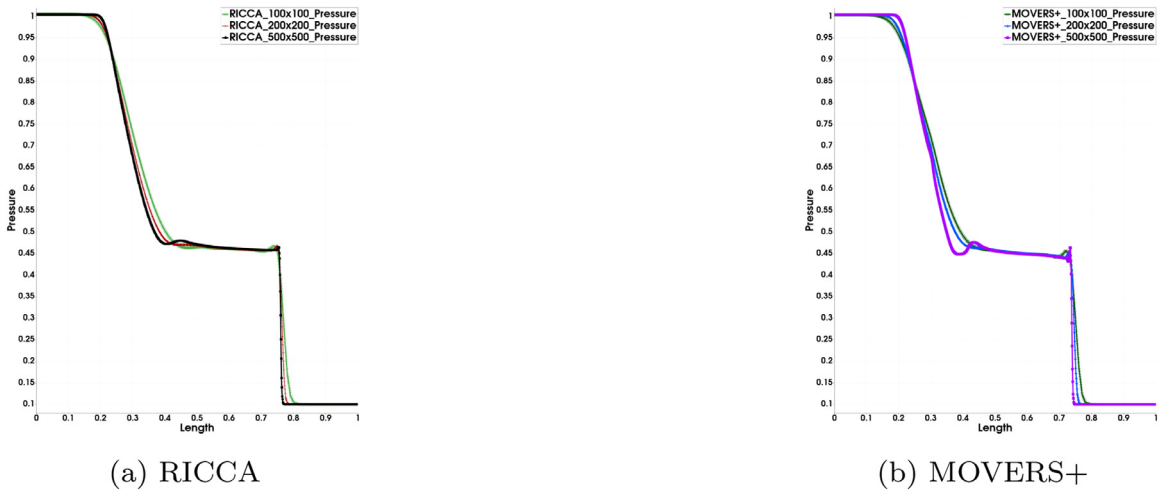

Fig. 19. Plot of Pressure at the centreline of the shock tube using MOVERS+ and RICCA.

7. Benchmark test cases for viscous flows

These test cases evaluate the ability of the algorithms discussed in sections (3) and (4) to resolve the viscous flow features especially shock and boundary layer interactions. The viscous terms are discretised using Green-Gauss method. The details of the discretisation strategies used can be found in [24].

7.1. Viscous shock tube test case

A comprehensive review of shock tube is presented in [21] and for detailed history of shock tube one can refer to [12]. Numerical simulations are carried out for viscous shock tube using MOVERS+ and RICCA. The primary objective is to check if the numerical schemes can resolve the boundary layers and the effect of these boundary layers on all the non-linear waves. The computational domain consists of a shock tube of length $L = 1$ with height to length ratio being given by $\frac{h}{L} = 0.3$. Sod shock tube data is considered for initial conditions with Reynolds number, $Re = 25000$ and Prandtl number, $Pr = 0.72$. Nonuniform stretched grids are used for resolving boundary layers and the following grid sizes ($101 \times 101, 201 \times 201$ and 501×501), are considered for the simulation and the results from the fine grid simulations are presented here.

Results obtained from second order accurate simulations are presented for both MOVERS+ and RICCA. Figure (18) depicts the density contours where shock, contact discontinuit and expansion fans are clearly resolved. Figure (19) shows the distribution of pressure on different grids at the centreline of the shock tube. The inviscid features of the flow field are captured well and the viscous features like the curved shock, boundary layer are resolved reasonably well.

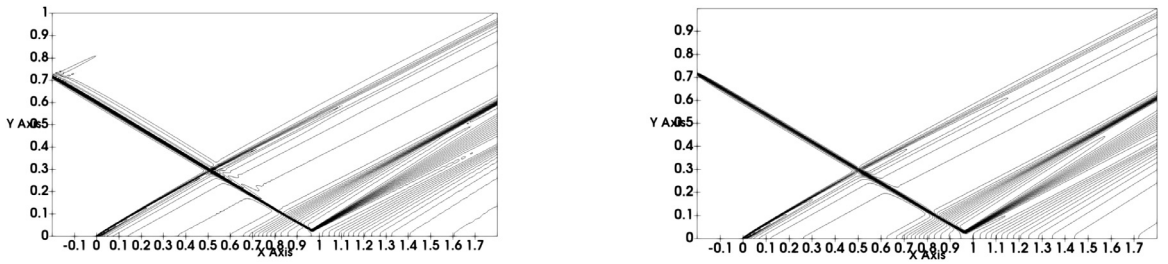

(a) Movers+ on 800 × 400 grid (b) RICCA on 800 × 400 Grid

Fig. 20. Pressure Contours of Shock Wave Boundary Layer Interaction .

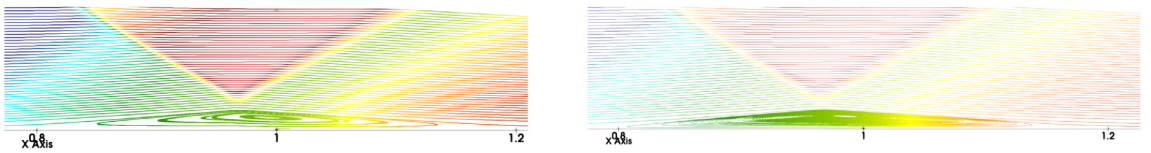

(a) Streamlines in recirculation zone using MOVERS+ (b) Streamlines in recirculation zone using RICCA

Fig. 21. Recirculation zone: streamlines.

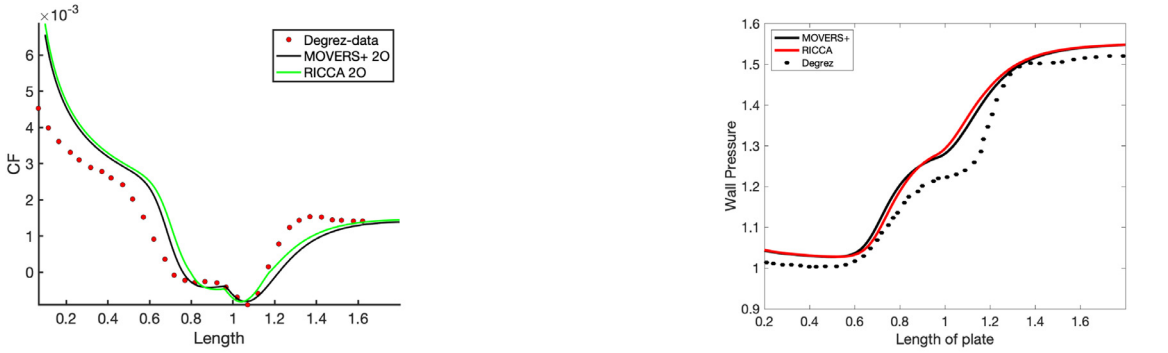

(a) 800 × 400 Grid (b) Wall Pressure on 800 × 400 grid

Fig. 22. Comparison of coefficient of skin friction and wall pressure using experimental data with MOVERS+ and RICCA.

7.2. Shock wave laminar boundary layer interaction (SWBLI)

This test case represents the interaction of an oblique shock wave with a laminar boundary layer. This is a standard test case to test the ability of the numerical schemes to resolve viscous features like flow separation, bubble formation and corresponding negative skin friction as explained in Hakkinen in [5], and the numerical simulations were performed by Degrez [1]. Figure (20) represents the pressure contours from MOVERS+ and RICCA respectively on 800 × 400 grid. It can be observed that the incident shock on to the boundary layer, the leading edge shock from the boundary layer, the reflected shock, the expansion fans and the recirculation bubble in the boundary layer are well resolved. The resolution of shocks is good in the case of MOVERS+ when compared to the RICCA. Further, the figure (21) shows the streamlines in the recirculation zone where the separation bubble is formed. The comparison of wall pressures, given by $\frac{p_w}{p_\infty}$, obtained with MOVERS+, RICCA, with the data of Degrez [1] is shown in Fig. (22 b). Both MOVERS+ and RICCA show the correct trend of the wall pressure but some deviation from the experiments is found. Fig. (22 a) refers to the coefficient of skin friction on the wall surface obtained by 800 × 400 grid. It is observed that, while both MOVERS+ and RICCA resolve the negative skin friction region, MOVERS+ gets the negative value of skin friction much better than RICCA even on coarser grid. Resolving the separation bubble and correspondingly obtaining the negative values of skin friction is very difficult and is possible only with second order accuracy together with basically low diffusive schemes and a proper grid which resolves the boundary layer well. The deviation of the skin friction coefficient with the experimental values away from the bubble region in both the schemes is probably due to the numerical diffusion present in the numerical schemes in smooth regions.

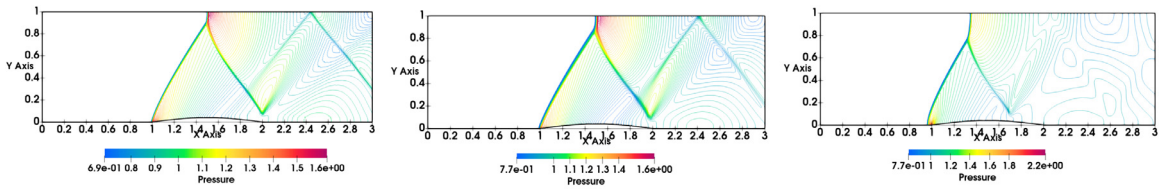

(a) MOVERS+ (b) RICCA (c) LLF

Fig. 23. Comparison of Pressure Contours for LLF, RICCA and MOVERS+ on 900 × 300 grid.

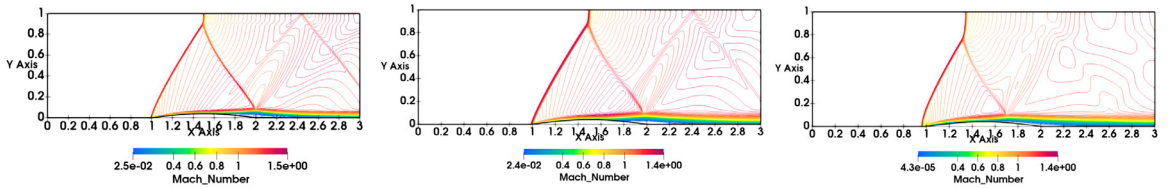

(a) MOVERS+ (b) RICCA (c) LLF

Fig. 24. Comparison of Mach Number Contours for LLF, RICCA and MOVERS+ on 900 × 300 grid.

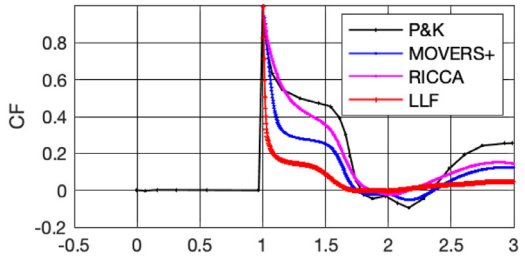

Fig. 25. CF Comparison of LLF, RICCA and MOVERS+ on 900 × 300 grid .

7.3. Viscous flow over a cylindrical bump in a channel

The third test case considered is a low supersonic viscous flow over a 4% thick circular bump in a channel. The test case details, boundary conditions and other flow features can be found in [22]. Numerical simulations are carried out using MOVERS+, RICCA and LLF. It can be seen from the figures (23,24) that a shock wave evolves from the leading edge of the bump. Since the top wall has only flow tangency condition, the shock wave just reflects from the wall. At the bottom wall, no-slip boundary condition gets enforced from the leading edge and hence the boundary layer starts growing. As the flow encounters the trailing edge of the bump, it separates, where the reflected shock impinges on the boundary layer and gets reattached in the downstream direction. These flow features are captured accurately by MOVERS+ while the numerical diffusion in RICCA leads to insufficient resolution. Figure (25) shows a comparison of the skin friction coefficient (CF) with the data taken from [22] on all the three grids. A very good match of skin friction coefficient obtained with MOVERS+ is observed near the separation region and on the initial part of the bump. There is some deviation of skin friction coefficient in the expansion regions. It can also be observed that RICCA does not show the separation region distinctively on a coarse grid but on fine grid the separation is evident. MOVERS+ consistently shows the separation region on all the three grids where as LLF is consistently poor in resolving the separation region.

This paper primarily deals with the robustness of the numerical schemes with perfect gas EOS and also with the applicability of the numerical schemes to the cases where stability of the shocks are of concern. It is worth noting that due to the independence of the schemes of the underlying eigen-structure of systems, simulations for flows with complex EOS and tabulated EOS can be easily done without any modification in the algorithms, which will be a significant advantage. Such applications, which are beyond the scope of this paper, will be presented elsewhere.

8. Summary

In this work, two simple central algorithms are presented. The first algorithm, RICCA, is based on generalized Riemann invariants for a contact discontinuity. This leads to the coefficient of numerical diffusion equaling the fluid velocity. This diffusion helps in resolving steady contact discontinuities exactly but is insufficient in resolving the shocks in a robust way. Therefore, an additional numerical diffusion based on sound speed is added, which is scaled with the sign function of pressure difference so that it goes to zero near steady contact-discontinuity. The second algorithm is based on a modification of

the previously introduced numerical diffusion matching RH conditions in a simple central solver. The modification removes the wave speed correction present in the previous version and leads to a very accurate scheme but too low in numerical diffusion. Hence an additional diffusion, taken from RICCA, is added with the help of a shock sensor. The resulting scheme, MOVERS+, is accurate and yet robust. The formulations for both the numerical schemes are simple, do not need any wave speed correction, independent of eigen-structure and do not need entropy fixes. These numerical schemes work well for various benchmark test cases involving shock instabilities and shock anomalies. Both the numerical schemes are capable of resolving steady contact-discontinuities exactly. Further, the first order solutions obtained by MOVERS+ on any grid are comparable with the second order results of RICCA. MOVERS+, though does not capture steady shocks exactly, has better shock capturing capabilities than RICCA. RICCA is less diffusive than the LLF scheme, is capable of capturing steady contact discontinuities exactly and hence can be a better alternative to LLF scheme. Further, numerical simulations of viscous 2D flows have been carried out using MOVERS+ and RICCA. As the boundary layer can be considered to be a set of slipstreams, these numerical schemes are expected to capture them accurately. However, MOVERS+ performed much better than RICCA for viscous flows especially in resolving flow separation bubbles. While the exact contact-discontinuity capturing feature of RICCA for inviscid flows led to accurate resolution of inviscid features, the excessive numerical diffusion in smooth regions has clearly affected the resolution of viscous regions.

Acknowledgment

The third author thanks Prof. Francois Dubois for some interesting and fruitful discussions.

References

[1] G. Degrez, C.H. Boccadorosand, J.F. Wendt, The interaction of an oblique shock wave with a laminar boundary layer revisited. an experimental and numerical study, J Fluid Mech 177 (1987) 247–263.
[2] V. Elling, The carbuncle phenomenon is incurable, Acta Math. Sci. 29 (6) (2009) 1647–1656.
[3] A. Harten, P.D. Lax, B. van Leer, On upstream differencing and godunov-type schemes for hyperbolic conservation laws, SIAM Rev. 25 (1) (1983) 35–61.
[4] K. Huang, H. Wu, H. Yu, D. Yan, Cures for numerical shock instability in *HLLC*solver, Int J Numer Methods Fluids 65 (9) (2011) 1026–1038.
[5] R.J. Hakkinen, I. Gerber, L. Trilling, S.S. Abarbanel, The interaction of an oblique shock wave with a laminar boundary layer, NASA Memorandum 2-18-59W.
[6] A. Jameson, Analysis and design of numerical schemes for gas dynamics 1: artificial diffusion, upwind biasing, limiters and their effect on accuracy and multigrid convergence, Journal of Computational Fluid Dynamics 4 (3–4) (1995) 171–218.
[7] A. Jameson, The present status, challenges, and future developments in Computational Fluid Dynamics, Technical report, 77th AGARD Fluid Dynamics Panel Symposium, 1996. CP-578
[8] S. Jaisankar, Raghurama Rao S.V, A central rankine-hugoniot solver for hyperbolic conservation laws, J Comput Phys 228 (3) (2009) 770–798.
[9] S. Jaisankar, Raghurama Rao S.V, Diffusion regulation for euler solvers, J Comput Phys 221 (2007) 577–599.
[10] A. Jeffrey, Lectures on Nonlinear Wave Propagation, in: G. Ferrarese (Ed.), Wave Propagation, Springer, 1980.
[11] S. Karni, S. Canic, Computations of slowly moving shocks, J Comput Phys 136 (1997) 132–139.
[12] P.o. Krehl, History of shock waves, explosions and impact: A chronological and biographical reference, Springer Science & Business Media, 2008.
[13] A. Kurganov, E. Tadmor, New high-resolution central schemes for nonlinear conservation laws and convection-diffusion equations, J Comput Phys 160 (1) (2000) 241–282.
[14] F. Kemm, Heuristical and numerical considerations for the carbuncle phenomenon, Appl Math Comput 320 (2018) 596–613.
[15] D.W. Levy, K.G. Powell, B. van Leer, Use of a rotated riemann solver for 2-dimensional Euler equations, J Comput Phys 106 (1993) 201–214.
[16] M.S. Liou, Mass flux schemes and connection to shock instability, J Comput Phys 160 (2) (2000) 623–648.
[17] M. Manna, A three dimensional high resolution upwind finite volume Euler solver, Technical note 180, Von Karman Institute for Fluid Dynamics, 1992.
[18] R.W. MacCormack, A perspective on a quarter century of CFD research, AIAA paper, 1993, No. AIAA-93-3291-CP.
[19] F. Moukalled, M. Darwish, A high-resolution pressure-based algorithm for fluids at all speeds, J Comput Phys 168 (2001) 101–133.
[20] N. Fleischmann, S. Adami, N.A. Adams, A shock-stable modification of the HLLC riemann solver with reduced numerical dissipation, J Comput Phys (2020).
[21] O. Popczyk, Investigation of the fluid flow physics of two and three dimensional micro scale shock wave propagation based on high resolution Godunov type FVM based in house code, Cranfield University, M.Sc thesis, 2018.
[22] V. Parthasarathy, Y. Kallinderis, Directional viscous multigrid using adaptive prismatic meshes, AIAA Journal 33 (1) (1995).
[23] J.J. Quirk, A contribution to the great Riemann solver debate, Int J Numer Methods Fluids 6 (1994) 555–574.
[24] Ramesh Kolluru, Novel, Robust and Accurate Central Solvers for Real, Dense and Multicomponent Gases, Department of Aerospace Engineering, Indian Institute of Science, Bangalore, India, 2019 Ph.D thesis.
[25] P.L. Roe, Characteristic-based schemes for the euler equations, Annural Review of Fluid Mechanics 18 (1986) 337–365.
[26] P.L. Roe, Shock capturing, chapter 6, handbook of shock waves, I, Academic Press, 2001, pp. 787–877.
[27] R.C. Ripley, F.-S. Lien, M.M. Yovanovich, Numerical simulation of shock diffraction on unstructured meshes, Computers & Fluids 35 (2006) 1420–1431.
[28] R. Ansorge, T. Sonar, Mathematical models of fluid dynamics: Modelling, theory, basic numerical facts - An introduction, second edition, Wiley-VCH, 2009.
[29] Y. Stiriba, R. Donat, A numerical study of post shock oscillations in slowly moving shock waves, An International Journal of Computers and Mathematics with Applications 46 (2003) 719–739.
[30] Toro, E.F. Riemann Solvers and Numerical Methods for Fluid dynamic- A Practical Introduction, Springer, 3rd edition
[31] N.V. Raghavendra, S.V. Raghurama Rao, A boltzmann scheme with physically relevant discrete velocities for Euler equations, to be published in Journal of Advances in Engineering Sciences and applied Mathematics, 2021.
[32] P. Woodward, P. Colella, The numerical simulation of two-dimensional fluid flow with strong shocks, J Comput Phys 54 (1984) 115–173.
[33] H. Yee, R. Warming, A. Harten, A High-resolution Numerical Technique for Inviscid Gas-dynamic Problems with Weak Solutions, in: Eighth International Conference on Numerical Methods in Fluid Dynamics, Springer, 1982, pp. 546–552.
[34] S. Zhang, C.-W. Shu, A new smoothness indicator for the WENO schemes and its effect on the convergence to steady state solutions, J Sci Comput 31 (1/2) (2007) 273–305.